JOURNAL OF CATALYSIS **170,** 227–235 (1997)
ARTICLE NO. CA971736

On the Nature of Nonframework Cations in a Zeolitic deNO$_x$ Catalyst: Cu-Mordenite

Martin P. Attfield,* Scott J. Weigel,† and Anthony K. Cheetham*,[1]

*Materials Department, †Chemistry Department, University of California, Santa Barbara, California 93106

Received October 8, 1996; revised March 20, 1997; accepted April 21, 1997

The locations of extra-framework Cu^{2+} cations in hydrated copper ion-exchanged mordenite (formula $Cu_{1.384}T_{48}O_2 \cdot 28H_2O$, space group *Cmcm*, $a = 18.1659(4)$ Å, $b = 20.375(1)$ Å, $c = 7.495(1)$ Å, $V = 2774.4(4)$ Å^3, $Z = 1$, $R = 5.13\%$) and its partially dehydrated analog (formula $Cu_{1.468}T_{48}O_2 \cdot 4.04H_2O$, space group *Cmcm*, $a = 18.0546(7)$ Å, $b = 20.298(2)$ Å, $c = 7.4772(3)$ Å, $V = 2740.2(3)$ Å^3, $Z = 1$, $R = 3.90\%$) have been determined from the analysis of room-temperature single-crystal X-ray data. Two copper sites were found in the hydrated sample: one in the elliptical 8-ring and the other in the center of the main 12-ring channel. Upon dehydration three copper sites were determined; one in the elliptical 8-ring, one above the 6-ring in the main channel and the last in the circular 8-ring that leads into the main channel. The low coordination, but high accessibility, of the latter two cation sites in the partially dehydrated sample provides a possible explanation for the high activity of mordenite and its related pentasil family members for nitrogen oxide decomposition. © 1997 Academic Press

INTRODUCTION

The removal of nitrogen oxides from automobile exhaust streams has been achieved successfully over the last three decades by use of the three-way catalytic converter (1). However, the increasing drive towards the implementation of lean-burn engines, which will render the three-way catalyst ineffective for NO_x emission, has exacerbated the need for a new effective deNO$_x$ catalyst. At the present time, transition metal-loaded pentasil zeolite catalysts have been found to display the highest activity towards the decomposition of nitrogen oxides (2, 3), although problems still exist for the practical utilization of these catalysts.

In general, it has been observed that the pentasil zeolites (ZSM-5, ferrierite, and mordenite), in particular ZSM-5, are the zeolite hosts that produce the deNO$_x$ catalysts with the greatest activity (2, 3). The particular transition metal exchanged zeolite that is the most active for deNO$_x$ depends on the reaction conditions being used. Cu-ZSM-5 has been found to be the most active for many reactions, including direct decomposition of NO to N_2 and O_2 (4, 5) and the selective catalytic reduction (SCR) of NO by certain hydrocarbons in the presence of excess oxygen (6–8). Other transition metal exchanged zeolites show significant activity for the same reactions and sometimes even greater activity. For example, Co-ferrierite is the most active catalyst for the decomposition in the presence of methane and excess oxygen (9).

To understand the high activity of these catalysts requires knowledge of the location and coordination of the cations in the zeolite. There are only two reported diffraction studies on the locations of extra-framework transition metal cations in the pentasil zeolites, both involving nickel in ZSM-5 (10, 11). The study of dehydrated Ni-ZSM-5 located one nickel site in the sinusoidal 10-ring channel and another within a small cage above the sinusoidal channel. Further information on the locations of the cations in these catalysts has been deduced from indirect spectroscopic measurements. Photoluminescence measurements of Cu^+ cations have identified four individual types of Cu^+ cation in reduced ZSM-5 and mordenite (12), whose population depends upon the Cu loading, the framework Si/Al ratio and the type of framework. Electron spin resonance spectroscopy (ESR) provides evidence for at least two distinct sites in dehydrated Cu-ZSM-5 (12–14) and Cu-mordenite (12, 15). The two sites in the former are believed to have square planar and square pyramidal coordination, although their exact nature is unclear. X-ray absorption near edge spectroscopy (XANES) and extended X-ray absorption fine structure (EXAFS) spectroscopy have shown the presence of Cu^{2+} cations in ZSM-5 catalysts that are isolated at low loadings but form dimers at higher loadings (16, 17). A similar result was found for high loadings of Cu-mordenite from EXAFS analysis (18).

Cu-mordenite materials have been found to be significantly more active than nonpentasil zeolite-based catalysts for many of the deNO$_x$ reactions discussed in the literature (19, 20). Mordenite is well known both in nature and as a synthetic material. The Si/Al ratio varies from 5 (in natural mordenite) to ~30 in synthetic zeolites. The structure was

[1] To whom correspondence should be addressed. E-mail: cheetham@iristew.ucsb.edu.

0021-9517/97 $25.00
Copyright © 1997 by Academic Press
All rights of reproduction in any form reserved.

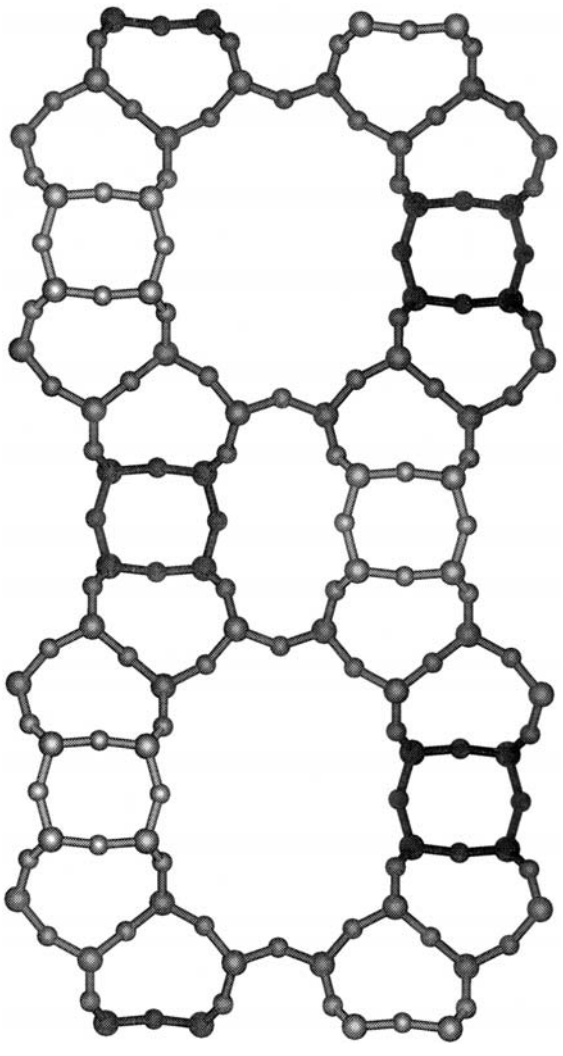

FIG. 1. The structure of mordenite viewed down the [001] direction.

first determined by Meier (21), but there is still a debate regarding the use of the centric or acentric space group for the structure (22). The framework of mordenite is based on 5-ring building units that are stacked in columns parallel to the [001] direction. The connection of these columns of 5-rings forms a near circular 12-ring channel (pore dimensions 6.5 by 7.0 Å) and an elliptical 8-ring channel (pore dimensions 2.6 by 5.7 Å) running along the [001] direction as shown in Fig. 1. Adjacent 12-ring and 8-ring channels are linked by circular double 8-rings. These double 8-rings are not aligned in the [100] direction, so a circular 8-ring channel is not formed in this direction. However, passage between adjacent 12-ring channels is possible by motion through the zig-zag channels (illustrated in Figs. 2a and 2b) which consist of two double 8-ring units on either side of the elliptical 8-ring channel. The only extra-framework cation locations reported for mordenite are those of the alkali and alkaline earth metals (23).

In this work we have used single crystal X-ray diffraction to probe the position and coordination of the copper cations in fully hydrated and partially dehydrated Cu-exchanged mordenite crystals in order to explain the high activity of these materials for deNO_x catalysis. It should be noted that, although a typical catalytic converter operates in an atmosphere containing ~10% water vapor, the degree of hydration of the zeolite catalyst under operating conditions is uncertain.

METHODS

Synthesis

The hydrothermal crystallization of the aluminosilicate mordenite was carried out in a Teflon-lined 23 ml Parr digestion bomb according to a modified version of the method used by Warzywoda (24). The reactants used were Davison 62 silica (Aldrich), sodium aluminate (Spectrum, 46.7 wt% Al_2O_3, 28.4 wt% Na_2O), sodium hydroxide (Fisher), and distilled water. The molar oxide composition of the gel was

$$4.32\ Na_2O : 19\ SiO_2 : Al_2O_3 : 294\ H_2O.$$

Pretreatment of the silica was necessary for the synthesis. The silica was first ground in a mortar and pestle before being placed in a preheated oven at 100°C. The silica was heated to 850°C in 30 min and held at this temperature for 20 h before being cooled to 100°C over a 12 h period. The sodium aluminate and NaOH were dissolved in 2/3 of the water and then passed through a 200 μm nylon filter. The silica was slurried with the remaining water before being added to the sodium aluminate solution. The resulting mixture was stirred for 20 min. The mixture was then placed in a digestion bomb and crystallized for 4 days at 180°C in a forced draft oven. After the hydrothermal treatment, the autoclave was removed from the oven and quenched in cold water. The resulting product was separated from the mother liquor by vacuum filtration, washed in deionized water, rinsed in acetone, and dried at room temperature. The product isolated from the synthesis contained two phases, mordenite and pollucite.

Fortunately, the two phases have distinct crystal morphologies and mordenite crystals could be identified with ease. The Na-mordenite crystals isolated from this synthesis had a chemical composition of $Na_{0.056}(Al_{0.066}Si_{0.934})O_2$ obtained from a crystallographic study (25). The Si/Al ratio (14.2) was obtained by using the Jones linear relationship (26) which relates the average T–O distance for each TO_4 unit to the Al-content in each TO_4 unit. Microprobe analysis on the hydrated Na-mordenite crystals gave a chemical composition ($Na_{0.068}(Al_{0.124}Si_{0.876})O_2$) with a rather lower Si/Al ratio of 7.1.

The mixture of products (mordenite and pollucite) was ion-exchanged in a 0.5 *M* $Cu(NO_3)_2$ (Aldrich) solution

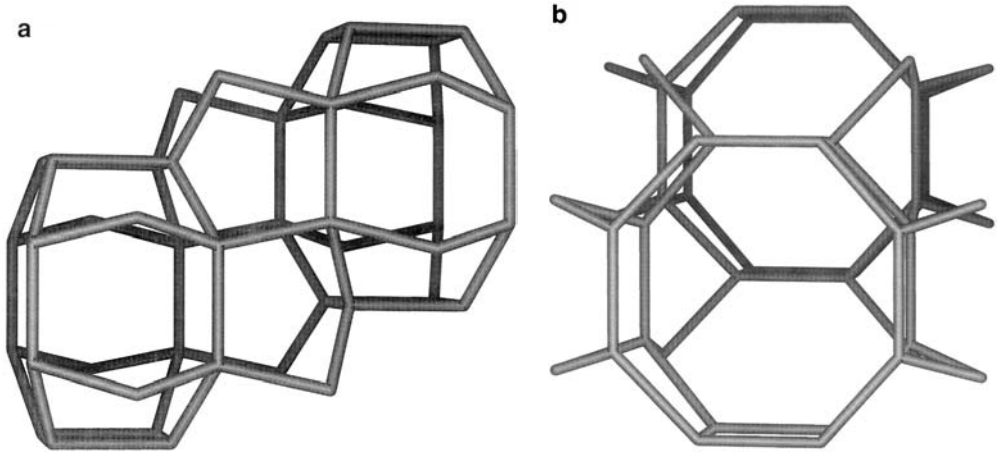

FIG. 2. The zigzag channel that connects the main 12-ring channels in mordenite viewed (a) side on and (b) end on. A stick representation is used for clarity.

(0.18 g of material per 40 mL of solution) for 24 days. The solution was refluxed throughout the whole period to aid ion-exchange. The sample was washed in 500 mL of deionized water at the end of the treatment. The mixture resulting from this procedure was blue in color. The chemical composition of the hydrated mordenite crystals given by microprobe analysis was $Cu_{0.051}Na_{0.008}(Al_{0.125}Si_{0.875})O_2$ and indicated that the Cu-exchange was 82% complete; the microprobe analysis was performed on a Cameca SX50 electron probe microanalyzer using a feldspar and copper metal as the standards. However, the structure determination (see below) points to a significantly higher Si/Al ratio, as was found for the as-synthesized sodium mordenite.

Crystal Structure Determination

Hydrated Cu-mordenite. A suitable single crystal for structure determination was mounted on a CAD4-MACH diffractometer, equipped with a Rigaku rotating anode source, and room temperature diffraction data were collected, the details of which, along with those of the refinement, are given in Table 1. The orthorhombic cell constants were determined from the positions of 25 centered reflections, found using a rotation photograph and optimized by least squares refinement; the resulting lattice parameters are given in Table 1. Two equivalent sets of data were collected in the ω-2θ scanning mode. Three standard reflections were monitored throughout the data collection; no significant variation in intensity was noted. The data were corrected for absorption using azimuthal Psi-scans (27). Data reduction were performed using the program RC85 (28).

The systematic absences were consistent with those of the orthorhombic space group *Cmcm* (#63). The mordenite framework structure reported in this space group (29) was used as the starting model for structure solution. All the extra-framework atoms were found from difference Fourier syntheses. Nine extra-framework electron density peaks were assigned as copper, oxygen, and silicon atoms. The extra-framework silicon atoms are part of the stacking fault in the (001) plane, as reported by Mortier (30). None of the remaining peaks in the final difference Fourier syntheses could be refined reasonably as atoms.

The T sites were considered to be solely occupied by Si atoms, as the Si/Al ratio of the framework was uncertain and inclusion of Al at the T sites did not improve the refinement significantly. The final cycle of least-squares refinement, against F, included the extinction parameter, atomic positions, anisotropic temperature factors for all atoms except the stacking fault T atoms, the isotropic temperature factor for the stacking fault T atoms, the occupancies of the extra-framework Cu atoms, and the T atoms involved in the stacking fault. The isotropic temperature factors for the stacking fault T atoms were constrained to have the same value. The occupancies of the extra-framework oxygen atoms were held at one, after refinement indicated that they had values close to or greater than one. Final fractional atomic coordinates, equalized temperature factors, and occupancies are given in Table 2. Selected bond distances are given in Table 3.

Partially dehydrated Cu-mordenite. A single crystal of hydrated Cu-mordenite was selected and placed at the bottom of a 0.1-mm diameter Lindemann glass capillary tube, the end of which had been tapered. The capillary tube was attached to a vacuum line and the region of the capillary containing the crystal was surrounded by a small heating coil. The crystal was heated from room temperature to 510°C under a vacuum of 10^{-5}–10^{-6} Torr (1 Torr = 133.3 $N\,m^{-2}$). The heating procedure included periods when the temperature was held constant at 100°C for 16 h, at 250°C for $8\frac{1}{2}$ h, at 450°C for 9 h, and at 510°C for 1 h. The crystal was cooled from 510°C to 475°C, where it was held at

TABLE 1

Crystallographic Data and Details of the Room Temperature Data Collection and Structure Refinement of Hydrated and Partially Dehydrated Cu-Mordenite

	Hydrated	Partially dehydrated
Formula	$Cu_{1.384}T_{48}O_{96} \cdot 28H_2O$	$Cu_{1.468}T_{48}O_{96} \cdot 4.04H_2O$
F_W	3476.42	3058.26
Crystal system	Orthorhombic	Orthorhombic
Space-group	*Cmcm* (#63)	*Cmcm* (#63)
F(000)	1760	1530
a (Å)	18.1659(4)	18.0546(7)
b (Å)	20.375(1)	20.298(2)
c (Å)	7.495(1)	7.4772(3)
V (Å^3)	2774.4(4)	2740.2(3)
Z	1	1
D_c	2.05 g cm^{-3}	1.84 g cm^{-3}
μ (cm^{-1})	68.50	67.00
Crystal shape	Hexagonal prism	Hexagonal prism
Crystal dimensions (mm)	0.05 × 0.05 × 0.04	0.075 × 0.05 × 0.03
Radiation	Cu Kα ($\lambda = 1.54180$ Å)	Cu Kα ($\lambda = 1.54180$ Å)
Absorption correction type	Psi scan	Psi scan
Absorption correction T min/T max	0.83/1.00	0.88/1.00
θ range (°)	0, 72	0, 72
hkl range	−1 to 22; −1 to 25; −9 to 9	−1 to 22; −1 to 25; −1 to 8
No. of reflections	6533	3459
No. of independent reflections	1520	1402
No. of observed reflections	1058	638
Criterion for reflection observation	$I > 3\sigma(I)$	$I > 2.5\sigma(I)$
R_{int}	3.13	2.23
No. of refined parameters	139	134
$\Delta\rho$ min/max (e Å^{-3})	−0.554/0.928	−0.440/0.399
$R(F)$ (%)	5.13	3.90
$R_w(F)$ (%)	6.39	4.66
S, goodness of fit	0.945	1.147
Extinction parameter	34(5)	9(2)
Weighting scheme	3-term Chebyshev	3-term Chebyshev

temperature for 36 h before being cooled to room temperature. A ramp rate of 1°C min^{-1} was used for all the heating and cooling steps. The capillary tube was sealed under vacuum at room temperature.

The crystal within the capillary tube was mounted on the diffractometer and room temperature diffraction data collected as described above, details of which, along with those of the refinement, are given in Table 1.

The systematic absences were again consistent with those of the orthorhombic space group *Cmcm* (#63). The mordenite framework structure obtained from the hydrated sample was used as the starting model for structure solution.

TABLE 2

Final Atomic Coordinates, Equalized Temperature Factors, and Occupancies of Hydrated Cu-Mordenite

Atom	*x*	*y*	*z*	*U*(eq) (Å^2)	Occupancy
T(1)	0.19595(5)	0.07347(4)	−0.0420(1)	0.0193	1.000
T(2)	0.30297(5)	0.19015(4)	0.0443(1)	0.0189	1.000
T(3)	0.08596(7)	0.11975(6)	0.2500	0.0152	0.949(6)
T(4)	0.41434(7)	0.22430(6)	−0.2500	0.0150	0.951(6)
O(1)	0.1227(2)	0.0883(2)	0.0725(4)	0.0440	1.000
O(2)	0.3769(2)	0.1935(2)	−0.0746(4)	0.0363	1.000
O(3)	0.2621(1)	0.1215(1)	0.0098(4)	0.0423	1.000
O(4)	0.0945(3)	0.1976(2)	0.2500	0.0434	1.000
O(5)	0.3291(3)	0.1935(2)	0.2500	0.0377	1.000
O(6)	0.1739(2)	0.0804(2)	−0.2500	0.0353	1.000
O(7)	0.2254(2)	0.0000	0.0000	0.0333	1.000
O(8)	0.2500	0.2500	0.0000	0.0407	1.000
O(9)	0.0000	0.0984(3)	0.2500	0.0300	1.000
O(10)	0.5000	0.2021(3)	−0.2500	0.0285	1.000
T(3sf)	0.083(2)	0.118(2)	−0.2500	0.041(8)	0.051(6)
T(4sf)	0.417(2)	0.222(2)	0.2500	0.041(8)	0.049(6)
Cu(1)	0.0000	0.0000	−0.5000	0.0714	0.156(8)
Cu(2)	0.5000	0.0030(9)	0.2500	0.1771	0.19(1)
O(1w)	0.0000	0.067(1)	−0.2500	0.1657	1.000
O(2w)	0.5000	0.190(2)	0.2500	0.1661	1.000
O(3w)	0.615(1)	0.010(2)	0.2500	0.3988	1.000
O(4w)	0.5000	0.074(2)	0.473(5)	0.3904	1.000
O(5w)	0.0000	0.183(2)	−0.2500	0.4521	1.000

TABLE 3

Selected Bond Distances (Å) in Hydrated Cu-Mordenite

T(1)–O(1)	1.611(3)	T(1)–O(3)	1.598(3)
T(1)–O(6)	1.616(1)	T(1)–O(7)	1.620(2)
Average T(1)–O bond length 1.611			
T(2)–O(2)	1.613(3)	T(2)–O(3)	1.604(3)
T(2)–O(5)	1.614(2)	T(2)–O(8)	1.5885(8)
Average T(2)–O bond length 1.605			
T(3)–O(1)	1.621(3)	T(3)–O(1)	1.621(3)
T(3)–O(4)	1.594(5)	T(3)–O(9)	1.621(2)
Average T(3)–O bond length 1.614			
T(4)–O(2)	1.608(3)	T(4)–O(2)	1.608(3)
T(4)–O(4)	1.599(5)	T(4)–O(10)	1.620(2)
Average T(4)–O bond length 1.609			
Weighted average T–O bond length 1.609			
Cu(1)–O(1w) × 2	2.32(1)	Cu(1)–O(9) × 2	2.744(4)
Cu(1)–O(1) × 4	2.917(4)	Cu(1)–Cu(1)	3.75
Cu(2)–O(3w) × 2	2.10(2)	Cu(2)–O(4w) × 2	2.22(3)
Cu(2)–O(4w) × 2	2.61(4)	Cu(2)–Cu(2)	3.750(1)
O(1w)–O(5w)	2.36(4)	O(1w)–O(6) × 2	3.170(5)
O(1w)–O(1) × 2	3.316(5)	O(1w)–O(9) × 2	3.37(2)
O(2w)–O(5w)	2.59(5)	O(2w)–O(4w) × 2	2.89(4)
O(2w)–O(5) × 2	3.106(5)	O(2w)–O(2) × 4	3.305(3)
O(3w)–O(4w) × 2	2.98(3)	O(3w)–O(4w) × 2	3.41(4)
O(3w)–O(7) × 2	3.46(2)		
O(4w)–O(4w)	3.06(7)	O(4w)–O(10) × 2	3.33(3)
O(4w)–O(4w)	3.35(7)	O(4w)–O(2)	3.39(2)

TABLE 4

Final Atomic Coordinates, Equalized Temperature Factors, and Occupancies of Partially Dehydrated Cu-Mordenite

Atom	*x*	*y*	*z*	*U*(eq) (Å^2)	Occupancy
T(1)	0.1963(1)	0.07322(7)	−0.0420(2)	0.0220	1.000
T(2)	0.3031(1)	0.19038(9)	0.0452(2)	0.0228	1.000
T(3)	0.0860(2)	0.1185(1)	0.2500	0.0183	0.973(7)
T(4)	0.4145(2)	0.2247(1)	−0.2500	0.0177	0.970(7)
O(1)	0.1226(3)	0.0863(3)	0.0734(7)	0.0435	1.000
O(2)	0.3765(3)	0.1938(3)	−0.0735(4)	0.0427	1.000
O(3)	0.2609(4)	0.1228(3)	0.0101(7)	0.0486	1.000
O(4)	0.0938(4)	0.1964(4)	0.2500	0.0436	1.000
O(5)	0.3294(4)	0.1936(5)	0.2500	0.0424	1.000
O(6)	0.1735(4)	0.0799(4)	−0.2500	0.0344	1.000
O(7)	0.2254(4)	0.0000	0.0000	0.0370	1.000
O(8)	0.2500	0.2500	0.0000	0.0532	1.000
O(9)	0.0000	0.0939(5)	0.2500	0.0348	1.000
O(10)	0.5000	0.2034(5)	−0.2500	0.0324	1.000
T(3sf)	0.085(7)	0.116(5)	−0.2500	0.04(2)	0.029(7)
T(4sf)	0.410(7)	0.235(5)	0.2500	0.04(2)	0.029(7)
Cu(1)	0.0000	0.0000	0.0000	0.0723	0.205(9)
Cu(2)	0.313(2)	0.042(2)	0.2500	0.0426	0.043(6)
Cu(3)	0.5000	0.152(4)	0.09(1)	0.0937	0.038(9)
O(1w)	0.0000	0.066(2)	−0.2500	0.1128	0.53(4)
O(2w)	0.5000	0.187(2)	0.2500	0.0708	0.48(5)

After refinement of the atomic coordinates and anisotropic temperature factors of the framework atoms, a total of seven extra-framework copper, oxygen, and silicon atoms were found from difference Fourier syntheses. None of the remaining peaks in the final difference Fourier syntheses could be refined reasonably as atoms. The final cycle of least-squares refinement, against *F*, included the same parameters as for the hydrated structure, in addition to the occupancies of the extra-framework oxygen atoms. The isotropic temperature factors for the stacking fault T atoms were again constrained to have the same value. Final fractional atomic coordinates, isotropic temperature factors, and occupancies are given in Table 4. Selected bond distances are given in Table 5.

All least-squares, Fourier, and subsidiary calculations for both structures were performed using CRYSTALS (31). Complex neutral atom scattering factors were taken from Ref. (32).

RESULTS

Hydrated Cu-mordenite. The formula given by the structural analysis is $Cu_{0.029}(Al_{0.065}Si_{0.935})O_2 \cdot 0.583H_2O$, which gives a Cu/T site ratio of 0.029. The Si/Al ratio (14.4) was obtained from the Jones linear relationship as mentioned previously (26). This indicates that most of the framework's negative charge is compensated by the copper cations, as expected, assuming the presence of Cu^{2+} cations in the structure. The values of the extra-framework cation/T site ratio and the Si/Al ratio are in excellent agreement to those obtained from the structural analysis on the Na-mordenite crystal (24), where the Na/T ratio (which should be double that of the Cu/T site ratio) is 0.056 and the Si/Al ratio is 14.2. Agreement with the composition given by the microprobe analysis is not so good, although we were unable to analyze the exact crystal for which X-ray data were collected.

The structure of the hydrated Cu-mordenite is shown in Fig. 3. Two Cu^{2+} cation sites were located in positions similar to those found in a hydrated Ca-exchanged mordenite (29). The first, Cu(1), is found to lie in the center of the elliptical 8-ring which forms part of the elliptical 8-ring channels. The Cu(1) cations are bound to two O(9) atoms at 2.744(4) Å and four O(1) atoms at 2.917(4) Å. Two water molecules, O(1w), at 2.32(1) Å complete the coordination environment, which is shown in Fig. 4 and may be described as a distorted hexagonal bipyramid. The Cu(1)–Oz (where Oz is a framework oxygen atom) distances are rather long for Cu^{2+} cations, so most of their coordination must come from the two water molecules bound to them. The presence of 46% of the exchanged Cu^{2+} cations in the Cu(1) site and their coordination to the Oz atoms indicates that the O(1) and O(9) framework atoms are undersaturated oxygen atoms belonging to Al-centered TO_4 units. This theory is supported by the fact that the T site (T(3)) to which O(1) and O(9) are bound has the longest average T–O bond length of the four T sites in the structure (see Table 3), implying that it contains the most aluminum.

The second Cu^{2+} cation, Cu(2), is situated in the center of the main channel, opposite an 8-ring that forms the end of the zig-zag passage. It is octahedrally coordinated by six

TABLE 5

Selected Bond Distances (Å) in Partially Dehydrated Cu-Mordenite

T(1)–O(1)	1.609(5)	T(1)–O(3)	1.589(5)
T(1)–O(6)	1.614(3)	T(1)–O(7)	1.607(3)
Average T(1)–O bond length 1.605			
T(2)–O(2)	1.597(5)	T(2)–O(3)	1.591(5)
T(2)–O(5)	1.604(3)	T(2)–O(8)	1.581(2)
Average T(2)–O bond length 1.593			
T(3)–O(1)	1.615(5)	T(3)–O(1)	1.615(5)
T(3)–O(4)	1.586(8)	T(3)–O(9)	1.631(4)
Average T(3)–O bond length 1.612			
T(4)–O(2)	1.614(5)	T(4)–O(2)	1.614(5)
T(4)–O(4)	1.609(8)	T(4)–O(10)	1.603(4)
Average T(4)–O bond length 1.610			
Weighted average T–O bond length 1.603			
Cu(1)–O(1w) × 2	2.30(2)	Cu(1)–O(9) × 2	2.670(7)
Cu(1)–O(1) × 4	2.875(6)		
Cu(2)–O(7) × 2	2.59(2)	Cu(2)–O(3) × 2	2.61(3)
Cu(3)–O(2) × 2	2.68(5)	Cu(3)–O(10)	2.75(9)
Cu(3)–Cu(3)	2.4(2)		
O(1w)–O(6) × 2	3.170(5)	O(1w)–O(1) × 2	3.316(5)
O(1w)–O(9) × 2	3.37(2)		
O(2w)–O(2) × 4	3.305(3)		

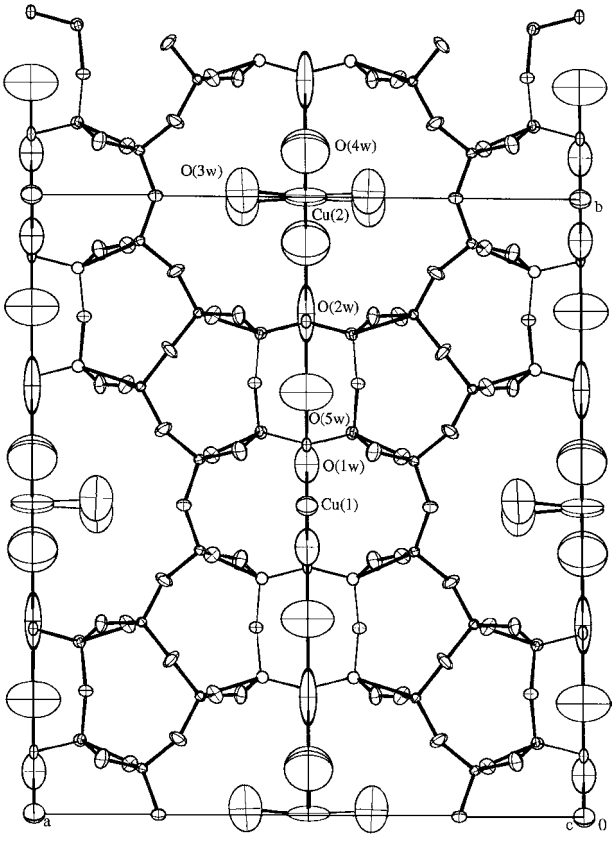

FIG. 3. The crystal structure of hydrated Cu-mordenite viewed along the [001] direction. Thermal ellipsoids are shown at 30% probability.

water molecules, two O(3w) atoms at 2.10(2) Å, two O(4w) atoms at 2.22 Å and two further O(4w) atoms at 2.61(4) Å. As can be seen from the Cu(2)–O(w) bond distances and the coordination geometry shown in Fig. 5, the $[Cu(H_2O)_6]^{2+}$ octahedra are Jahn–Teller distorted in a *cis* fashion. Similar *cis* Jahn–Teller distortions are seen for other Cu^{2+} complexes, particularly those with bidentate ligands; for example, $[Cu(bipyr)_2NO_2]NO_3$ has four short Cu–N bond lengths

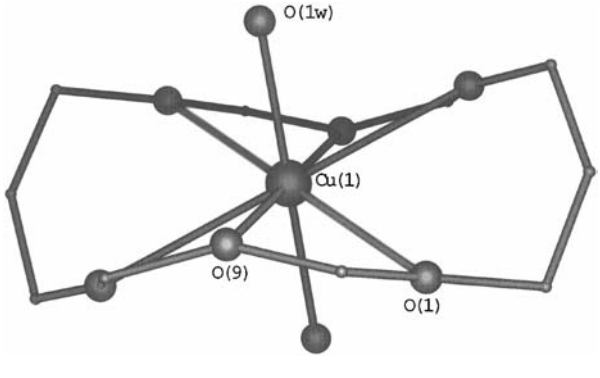

FIG. 4. The coordination environment of Cu(1) in the elliptical 8-ring. Only the oxygen atoms coordinated to the Cu^{2+} cations are shown.

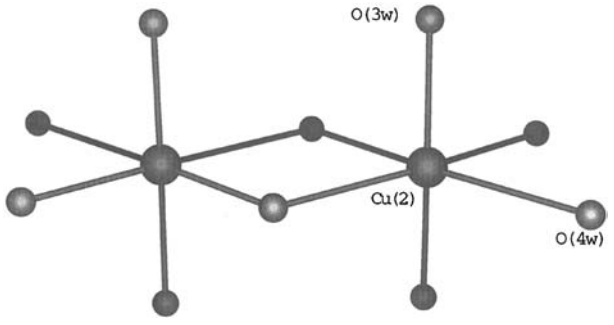

FIG. 5. An illustration of the distorted octahedral environment of Cu(2) by water molecules. The formation of the dimer shown occurs when two adjacent Cu(2) sites are occupied.

in the range 1.99 to 2.08 Å to the bidentate bipyridine ligands and two longer *cis* Cu–O bonds of 2.24 and 2.33 Å to the nitrite group (33). The four shorter Cu(2)–O bond lengths and the Cu(1)–O(1w) distances are in agreement with those found for other aqueous Cu^{2+} species, for example, $Cu(ClO_4)_2 \cdot 6H_2O$ (34), where the bond lengths to the oxygen atoms of the water molecule are 2.09 Å, 2.16 Å, and 2.28 Å. The $[Cu(H_2O)_6]^{2+}$ octahedra may share edges, as shown in Fig. 5, to form dimers in the main channel; however, due to the low occupancy of the Cu(2) site this is likely to be a rare occurrence. Presumably, occupation of the channel intersection is favored for the $[Cu(H_2O)_6]^{2+}$ cations as it is less spatially confined and entropically favorable.

Two additional water molecules, O(2w) and O(5w), were found in the structure, neither being directly bound to the Cu^{2+} cations. These water molecules are close enough to hydrogen bond to each other and the waters bound to the Cu^{2+} cations. The 99result of the intermolecular interactions is the formation of a hydration complex ...Cu(1)–O(1w)–O(5w)–O(2w)–O(4w)–Cu(2)–O(4w)–O(2w)–O(5w)–O(1w)–Cu(1)... along the *b* axis (see Fig. 3), in addition to the hydration complex formed along the *c* axis through interactions of the Cu(2) complexes linked by O(4w). The occupancy of the water sites is much higher than that required to form the Cu^{2+} complexes, indicating that the water molecules must be partially localized in these positions by hydrogen-bonding interactions with other water molecules and the Oz atoms. The bond distances of the water molecules to the other water molecules and Oz atoms are given in Table 3 and are all of reasonable values to allow for the aforementioned possibility. The high values of the temperature factors of the extra-framework water molecules suggest there is a lot of positional and thermal disorder of these species. Under these circumstances we were unable to refine the occupancies of the water molecules, even though some of them should be less than one to avoid the chemically unreasonable close contacts to the framework atoms involved in formation of the stacking fault planes, T(3sf) and T(4sf).

Partially dehydrated Cu-mordenite. The formula given by the structural analysis is $Cu_{0.031}(Al_{0.040}Si_{0.960})O_2 \cdot 0.084H_2O$, which gives a Cu/T site ratio of 0.031. This is in excellent agreement with the Cu/T ratio of 0.029 found for the hydrated Cu-mordenite sample. The Si/Al ratio of 25.2 given by the Jones relationship (26) is rather high in comparison to the hydrated structure (Si/Al = 14.4). The lower values of the average T–O bond lengths and, hence, the higher value of the Si/Al ratio, have been noted in other comparisons of hydrated and dehydrated zeolite structures (35) and result from the strong influence of the thermal parameters on the observed bond lengths (35, 36). The larger thermal parameters of the framework atoms in dehydrated structures arise from the presence of greater static disorder in these systems. Even though the average T–O bond length for each T site is reduced in the partially dehydrated structure, the longest average T–O bond length is still that of the T(3) site, implying that it still has the highest percentage occupation of Al and will have the most under-saturated Oz atoms around it.

The structure of the partially dehydrated Cu-mordenite is shown in Fig. 6. Three Cu^{2+} cation sites were located. The first, Cu(1), is again found to lie in the center of the elliptical 8-ring. The Cu(1) cations are bound to two O(9) atoms at 2.670(7) Å and four O(1) atoms at 2.875(6) Å. Two water molecules, O(1w), at 2.30(2) Å complete the coordination, which is shown in Fig. 4 and may be described as a distorted hexagonal bipyramid. The coordination of Cu(1) is exactly the same as that in the hydrated structure; however, in this structure the occupancy of the O(1w) site is much closer to the stoichiometric amount needed to coordinate all the Cu^{2+} cations. This site is the same as that found for Ca^{2+} cations in a dehydrated Ca-mordenite structure (35), in which no water in the O(1w) position remains, suggesting that when fully dehydrated the Cu^{2+} cations may well remain in this site. The presence of the extra-framework water O(1w) and O(2w) is surprising after the thermal treatment experienced by the crystal. The second Cu^{2+} cation, Cu(2), is situated above a 6-ring in the main 12-ring channel, where it is coordinated by two O(7) atoms at 2.59(2) Å and two O(3) atoms at 2.61(3) Å. The last and lowest occupied Cu site, Cu(3), is found to one side of the circular 8-ring that leads to the 12-ring channel. The Cu(3) atoms are bound to two O(2) atoms at 2.68(5) Å and one O(10) atom at 2.75(9) Å. The environments of Cu(2) and Cu(3) are shown in Figs. 7a and 7b, respectively. The occupancies of all the extra-framework species are low enough to assume that adjacent extra-framework sites, too close together to be physically reasonable, are not occupied simultaneously.

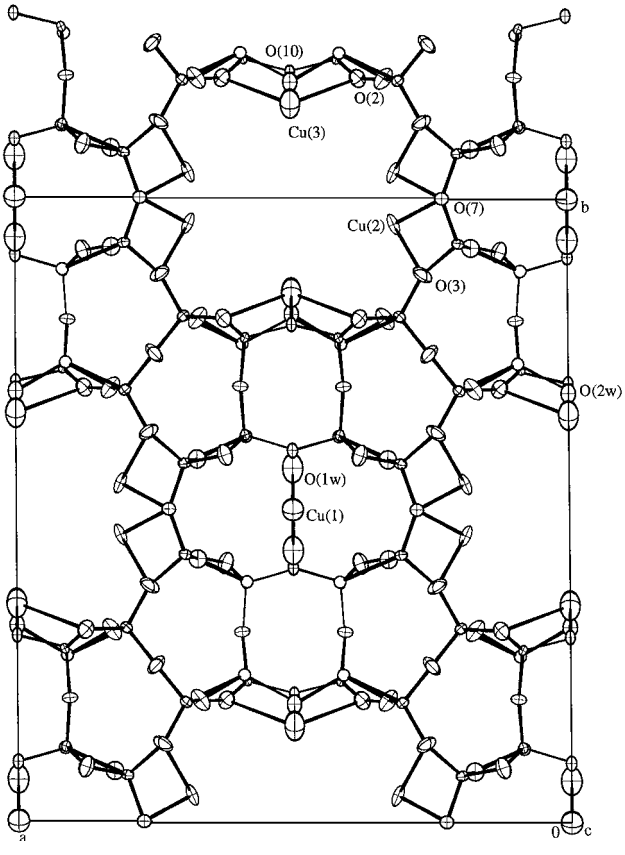

FIG. 6. The crystal structure of partially dehydrated Cu-mordenite viewed along the [001] direction. Thermal ellipsoids are shown at 30% probability.

The Cu–Oz bond lengths of all three Cu sites are rather long (2.59–2.875 Å), compared to those for other Cu^{2+} cation-containing zeolites, for example, Cu-zeolite-A (Cu–O distances 2.138 Å) (37) and Cu-chabazite (Cu–O distance 1.965 Å) (38). However, longer Cu–Oz bond lengths are found for some sites in Cu-faujasite (39), for example, 2.68 Å for the SI site, 2.56 Å for the SI' site, and 2.51 Å for the SII site, where interaction with residual water is thought to be taking place for the latter sites. The long Cu–Oz bond lengths may arise from three effects. One is due to X-ray diffraction only giving the average bond distance over many unit cells, so for a low occupancy site like those considered here, the Cu–Oz bond will appear longer on average than at the actual site where a Cu^{2+} cation is located. The second effect that might make the Cu–Oz bond lengths longer than normal is chemical in origin and results from the lone pairs on each of the Oz atoms not being directed ideally for bonding overlap. This means the Cu^{2+} cation will have to adjust its position to maximize the interaction with the lone pairs of the Oz atoms and may move further away than normally seen to optimize the bonding interaction. The third effect, as discussed for Cu-faujasite (39), involves residual water molecules stabilizing the Cu^{2+} cations, reducing their interaction with the Oz atoms. The residual water molecules would be undetectable as they are few in number, disordered, and oxygen scatters X rays weakly.

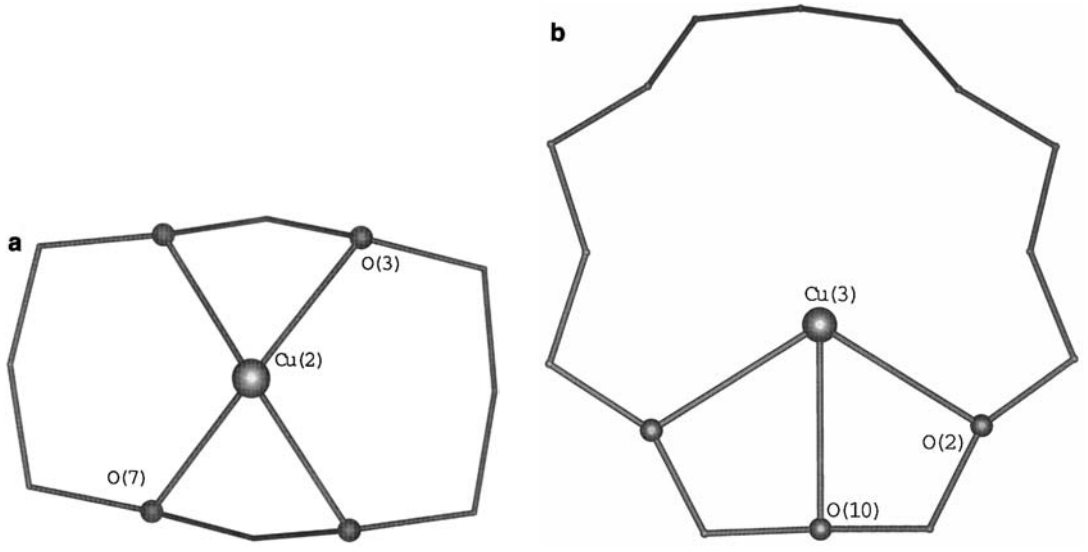

FIG. 7. The coordination environment of (a) Cu(2) above a 6-ring in the main 12-ring channel and (b) Cu(3) in the circular 8-ring adjacent to the main 12-ring channel. Only the framework oxygen atoms closest to the cation sites are shown for clarity.

All three Cu sites are similar to those found for a dehydrated Ca-mordenite studied by Mortier (35, 40), with the same order of occupancy, i.e., Cu(1) > Cu(2) > Cu(3), and bond distances longer than expected for Ca–Oz interactions. The Ca sites in dehydrated Ca-mordenite were used as the basis to calculate the ESR *g*- and *A*-values and the *d–d* transitions in the diffuse reflectance spectra of a dehydrated Cu-mordenite by Schoonheydt (15). They found that the best agreement between the experimental and theoretical values for the various parameters was achieved when the Cu^{2+} cations occupied the Cu(1) and Cu(2) sites, which is in agreement with this study as these two sites have the highest occupancy. The assumption that the copper remains as Cu^{2+} cations in this structure is made because the three copper sites are the same as those found for other divalent cations (35, 40) and the previously mentioned ESR study (15) showed that Cu^{2+} cations occupy two of the sites found in this diffraction study.

DISCUSSION

This study has located two Cu^{2+} cation sites in hydrated Cu-mordenite and the three sites produced when the system is partially dehydrated. For the partially dehydrated Cu-mordenite, the Cu^{2+} cations in the Cu(1) site are in the same location as the hydrated Cu-mordenite structure. The cations in the Cu(2) and Cu(3) sites result from the dehydration of the $[Cu(2)(H_2O)_6]^{2+}$ complex found in the main channel in the hydrated structure. On removal of the water molecules most of the Cu^{2+} cations migrate to the closest regions of the framework to find the highest possible coordination environment available to replace the water lost through dehydration. The positions we have found for the Cu^{2+} cations require the least movement and are likely to be occupied readily. Some of the Cu^{2+} cations migrate further from the initial position of the hydrated Cu^{2+} species to the Cu(1) site in the elliptical 8-ring which is presumably the favored cation site, as found for Na and Ca cations (23).

The location of the Cu^{2+} cations in the partially dehydrated Cu-mordenite means that they are poorly coordinated and open to interaction with NO and other molecules from more than one side. Such interaction is essential for all deNO_x mechanisms proposed. The low coordination of the Cu^{2+} cations makes them much more susceptible to redox chemistry, when exposed to NO, than a more highly coordinated Cu^{2+} cation, such as those found in the double 6-ring in faujasite (SI site), or even the SI' and SII sites (39, 41).

The positioning of the Cu^{2+} cations in the zeolite also affects their accessibility with regards to the reactant molecules passing through the zeolite pore structure; the greater the accessibility, the more conceivable it is that the exchanged zeolite will be an active catalyst. The accessibility of the Cu(2) and Cu(3) sites of the partially dehydrated Cu-mordenite are both high as they are in the main channel or in an 8-ring that forms part of the wall of the main channel. All reactant molecules entering the zeolite will be able to interact with the Cu^{2+} cations in these sites. The Cu(1) site in mordenite is less accessible to reactant molecules. Passage of gas molecules down the elliptical 8-ring channel is less likely than the main 12-ring channel due to its smaller pore dimensions and the fact that the presence of one cation in the Cu(1) site makes access to the remaining cations in the channel difficult. Access to the Cu(1) site through the main channel then the double 8-ring will be

low as this route is tortuous in comparison with movement straight down the 12-ring channel.

The presence of poorly coordinated, but highly accessible, Cu^{2+} cations provides a possible explanation for the high activity of Cu-mordenite materials in $deNO_x$ catalysis. The above reasoning may be extended to other zeolites in the pentasil family which are extremely active $deNO_x$ catalysts. For example, ZSM-5 has few cation sites within small inaccessible cavities in its structure and so it will render most of the extra-framework transition metal cations poorly coordinated and highly accessible to the reactant molecules. This line of reasoning also explains why the Cu-exchanged faujasite (*X* and *Y*) catalysts are relatively inactive towards $deNO_x$ catalysis. The majority of Cu^{2+} cations in these systems are found within the sodalite cage or double 6-ring (39, 41) where they are relatively well coordinated and inaccessible, even to molecules as small as NO itself.

ACKNOWLEDGMENTS

The work was funded by the MRL program of the National Science Foundation Award DMR 9123048 and by Los Alamos National Laboratory.

REFERENCES

1. Bond, G. C., "Heterogenous Catalysis, Principles and Applications." Oxford Univ. Press, Oxford, 1987.
2. Shelef, M., *Chem. Rev.* **95**, 209 (1995).
3. Iwamoto, M., and Mizuno, N., *J. Automot. Eng. [part D Proc. Inst. Mech. Eng.]* **207**, 23 (1993).
4. Iwamoto, M., Furukawa, H., Mine, Y., Uemura, F., Mikuriya, S., and Kagawa, S., *J. Chem. Soc. Chem. Commun.*, p. 1273 (1986).
5. Li, Y., and Hall, W. K., *J. Phys. Chem.* **94**, 6145 (1990).
6. Iwamoto, M., Yahiro, H., Shundo, Y., Yu-u, Y., and Mizuno, M., *Shokbai (Catalyst)* **32**, 430 (1990).
7. Iwamoto, M., and Hamada, H., *Catal. Today* **10**, 57 (1991).
8. Held, W., Konig, A., Richter, T., and Puppe, L., *Soc. Aut. Eng.*, Paper 900496, 1990.
9. Li, Y., and Armor, J. N., *Appl. Catal. B: Environmental* **3**, L1 (1993).
10. Mentzen, B. F., Sacerdote-Peronnet, M., and Bouix, J., *C.R. Acad. Sci., Paris* **315**, 1073 (1992).
11. Zhenyi, L., Wangjin, Z., Qin, Y., and Guanglie, L., *Stud. Surf. Sci. Catal.* **28**, 415 (1986).
12. Dedecek, D., Sobalik, Z., Tvaruzkova, Z., Kaucky, D., and Wichterlova, B., *J. Phys. Chem.* **99**, 16327 (1995).
13. Kucherov, A. V., Slinkin, A. A., Kondratev, D. A., Bondarenko, T. N., Rubenstein, A. M., and Minachev, Kh. M., *Zeolites* **5**, 320 (1985).
14. Sendoda, Y., and Ono, Y., *Zeolites* **6**, 209 (1986).
15. de Travernier, S., and Schoonheydt, R. A., *Zeolites* **11**, 155 (1991).
16. Grünert, W., Hayes, N. W., Joyner, R. W., Shapiro, E. S., Rafiq, M., Siddiqui, H., and Baeva, G. N., *J. Phys. Chem.* **98**, 10832 (1994).
17. Hamada, H., Matsubayashi, N., Shimaa, H., Kintaichi, Y., Ito, T., and Nishijima, A., *Catal. Lett.* **5**, 189 (1990).
18. Kuroda, Y., Kotani, A., Maeda, H., Moriwaki, H., Morimato, T., and Nagao, M., *J. Chem. Soc., Faraday Trans.* **88**, 1583 (1992).
19. Iwamoto, M., Yahiro, H., and Mizuno, N., *in* "Proceedings of the 9th International Zeolite Conference, Montreal 1992" (R. von Ballmoos, J. B. Higgins, and M. M. J. Treacy, Eds.), Vol. 2. p. 397. Butterworth-Heinemann, Stoneham, 1993.
20. Kim, M. H., Nam, I., and Kim, Y. G., *Appl. Catal. B* **6**, 297 (1995).
21. Meier, W. M., *Z. Kristallogr.* **115**, 439 (1961).
22. Alberti, A., Davoli, P., and Vezzalini, G., *Z. Kristallogr.* **175**, 249 (1986).
23. Mortier, W. J., "Compilation of Extra-framework Sites in Zeolites." Butterworth, Guildford, 1982.
24. Warzywoda, J., Dixon, A. G., Thompson, R. W., and Sacco, A., *J. Mater. Chem.* **5**, 1019 (1995).
25. Campbell, B. M., Gabriel, J.-C., and Cheetham, A. K., private commuication.
26. Jones, J. B., *Acta Crystallogr. B* **24**, 355 (1968).
27. North, A. C. T., Phillips, D. C., and Mathews, F. S., *Acta Crystallogr. A* **24**, 351 (1968).
28. Baird, P. D., "RC85," Chemical Crystallography Laboratory, Oxford, 1987.
29. Mortier, W. J., Pluth, J. J., and Smith, J. V., *Mat. Res. Bull.* **11**, 15 (1976).
30. Mortier, W. J., Pluth, J. J., and Smith, J. V., *Mat. Res. Bull.* **10**, 1319 (1975).
31. Watkin, D. J., Carruthers, J. R., and Betteridge, P. W., "CRYSTALS User Guide." Chemical Crystallography Laboratory, Oxford, 1990.
32. "International Tables for X-ray Crystallography" (T. Hahn, Ed.), Vol. IV. Kynoch, Birmingham, UK, 1984.
33. Porter, I. M., and Stephens, F. S., *J. Chem. Soc. (London) A*, 1248 (1969).
34. Mani, V. N., and Ramaseshan, S., *Z. Kristallogr.* **115**, 97 (1961).
35. Mortier, W. J., Pluth, J. J., and Smith, J. V., *Mat. Res. Bull.* **10**, 1037 (1975).
36. Liebau, F., "Structural Chemistry of Silicates." Springer, Heidelberg, 1985.
37. Lee, S. H., and Seff, K., *J. Phys. Chem.* **85**, 3978 (1981).
38. Pluth, J. J., Smith, J. V., and Mortier, W. J., *Mat. Res. Bull.* **12**, 1001 (1977).
39. Maxwell, I. E., and de Boer, J. J., *J. Phys. Chem.* **79**, 1875 (1975).
40. Mortier, W. J., *J. Phys. Chem.* **81**, 1334 (1977).
41. Gallezot, P., Ben Taarit, Y., and Imelik, B., *J. Catal.* **26**, 295 (1972).